A Force Feedback Teleoperated Needle Insertion Device for Percutaneous Procedures

O. Piccin, L. Barbé, B. Bayle, M. de Mathelin and A. Gangi

The International Journal of Robotics Research 2009 28: 1154 originally published online 19 May 2009
DOI: 10.1177/0278364909101408

A Force Feedback Teleoperated Needle Insertion Device for Percutaneous Procedures

O. Piccin
L. Barbé
B. Bayle
M. de Mathelin

LSIIT-IRCAD,
1, place de l'Hôpital,
University of Strasbourg,
Strasbourg 67091,
France
olivier.piccin@insa-strasbourg.fr
{barbe, bernard, demath}@eavr.u-strasbg.fr

A. Gangi

Radiology Department B,
University Hospitals of Strasbourg,
Strasbourg 67091,
France

Abstract

A novel robotized tool for percutaneous interventions under CT-scanner guidance is presented in this paper. This teleoperated compact robotic device can be used as an end-effector for an image-guided positioning robot. It is fully compatible with computed tomography constraints. In particular, it is able to manipulate needles that are longer than the overall height of its body. This novel device mimics the manual gesture performed by the physician by grasping and re-grasping the needle. This operating principle enables direct force measurement on the inserted surgical needle and allows efficient teleoperation with force feedback. In the paper, the specifications of this needle driver are presented and the proposed design is explained. Experiments conducted on swine under operating conditions were performed in order to validate both the concept and the design of the proposed insertion device in the context of teleoperated needle insertions with force feedback.

KEY WORDS—medical robots and systems, human-centered and life-like robotics, mechanics, design and control, telerobotics, simulation, interfaces and virtual reality.

The International Journal of Robotics Research
Vol. 28, No. 9, September 2009, pp. 1154–1168
DOI: 10.1177/0278364909101408

Figures 1, 2, 5–9, 12, 13 appear in color online: http://ijr.sagepub.com

1. Introduction

Computed tomography (CT) imaging is used widely for medical diagnosis and treatment. CT-guided interventional procedures are minimally invasive percutaneous techniques which limit patient trauma while ensuring a good targeting accuracy (Rösch et al. 2003). Figure 1 depicts a typical percutaneous procedure setup in which the patient is installed on the CT-scanner table and an initial scan is carried out to locate the intervention site and plan the insertion trajectory in order to determine the entry point and the incidence angle for the needle. The insertion is then performed gradually by the physician between two successive scans of the patient to check the needle position. It should be noted that in the absence of visual feedback the physician makes extensive use of haptic feedback to feel the anatomic structures during needle insertion. This iterative procedure is time consuming and leads to repeated exposures to X-rays for practitioners. This naturally limits the number of possible interventions which represents a drawback for patient care. For this reason, the design of a teleoperated robotic system to remotely insert needles under CT-guidance appears to be an adequate solution to protect the physician. Moreover, this may increase the number of such percutaneous procedures and lead to the development of the technique.

The general layout for a teleoperated robotized percutaneous procedure is depicted in Figure 2. It presents a master/slave teleoperation scheme which allows the medical staff to be protected. A robotic device located at the patient side in the CT-scanner room is operated from a radiation-shielded

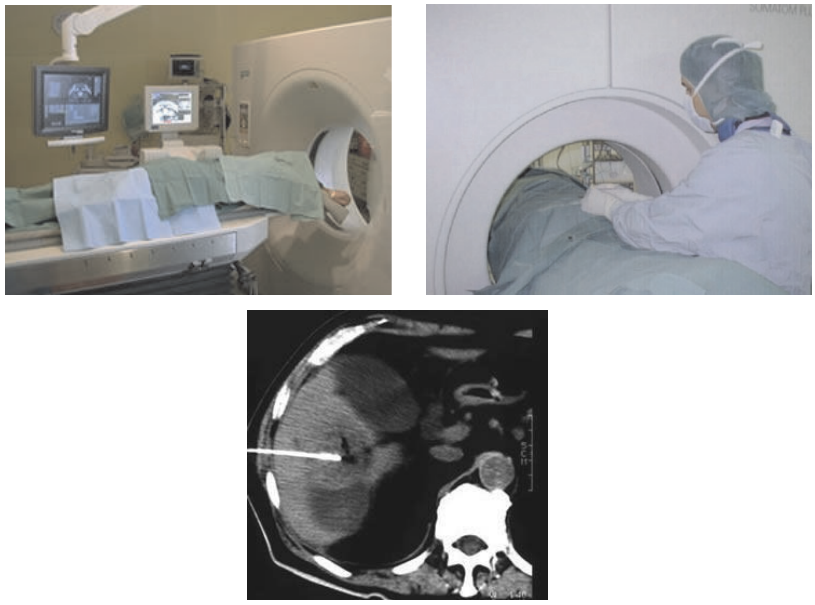

Fig. 1. Percutaneous procedure under CT guidance.

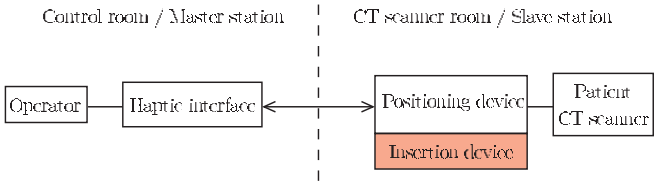

Fig. 2. General layout for a teleoperated percutaneous procedures.

control room by the radiologist who applies desired motions to a master device.

Ideally, this teleoperation has to be bilateral so that the practitioner installed at the master station is able to feel the forces that the needle mounted on the slave robot applies on the environment. Indeed, during percutaneous procedures, CT guidance is generally not sufficient to perform the insertion task. Since CT-scan acquisitions are only performed occasionally, real-time haptic feedback is highly desirable: this allows the needle insertion to be performed in a safer way and with high accuracy. For instance, it allows the successive punctures of the tissues to be detected which provide characteristic information regarding the progress of the needle (Barbé et al. 2007a).

It is possible to classify robotic systems for interventional radiology into two main categories (Cleary et al. 2006): (i) operating table-mounted systems; and (ii) patient-mounted systems. The first category includes the AcuBot and the MrBot, both from the Johns Hopkins University (Stoianovici et al. 2003; Patriciu et al. 2007), the commercial system Innomotion, from Innomedic GmbH (http://www.innomedic.de/), and the B-Rob robots, developed at the ARC Seibersdorf Research (Kettenbach et al. 2005). In the second category of systems, the robot is placed directly on the patient's body. Examples include LPR, from the TIMC-IMAG laboratory (Taillant et al. 2004), the UMI, from Tokyo University (Hong et al. 2004), the CT-Bot (Maurin et al. 2004) developed at the LSIIT Laboratory from the University of Strasbourg, and the Robopsy system, designed at the MIT (Barrett et al. 2005). In a different application area, the MARS robot is affixed directly to the patient's skull to achieve neurological percutaneous interventions (Shoham et al. 2003). The main characteristics of these systems are given in Table 1.

Whatever the proposed mechanical architecture, there is a general consensus that needle insertions have to be divided into two phases for safety reasons: (i) the initial positioning and orientation of the needle to target the anatomical target through the entry point on the skin; (ii) the insertion of the needle, followed by its extraction. Whereas there exist several positioning systems for CT use, some of them serve only as guides, with the insertion being performed manually, so this does not prevent X-ray exposure. The working principle of actuated needle insertion devices is often based on friction: opposing rollers act on the needle shaft to perform insertion or extraction (Stoianovici et al. 1997; Hong et al. 2004; Barrett et al. 2005). In this case, the traction on the needle shaft is highly dependent on the friction conditions, which are not controlled precisely. Furthermore, the needle displacement and grasping are combined, so that the insertion force can only be measured using indirect means with some uncertainty since friction ef-

Table 1. Characteristics of existing interventional radiology robots. (IG, image guidance; TEL, teleoperation; Ph, phantom validation; IV, *in vivo* validation; TM, table mounted; PM, patient mounted.)

System	Location	Imaging	Motion	Validation	Type	Insertion
AcuBot	JHU	CT	IG, TEL	IV	TM	Friction
MrBot	JHU	CT, MRI	IG	Ph	TM	Pneumatic
B-Rob II	ARC	CT	IG	IV	TM	Manual
Innomotion	Innomedic	CT, MRI	IG	IV	TM	Manual
LPR	TIMC	CT, MRI	IG	IV	PM	Pneumatic
CT-Bot	LSIIT	CT	IG	Ph	PM	Manual
Robopsy	MIT	CT	IG	Ph	PM	Friction
UMI	Tokyo University	US	IG	IV	PM	Friction
MARS	Jerusalem University	CT, MRI	IG	IV	PM	Manual

fects due to tissue adhesion and damping cannot be isolated. Consequently, it is difficult to obtain the precise force measurement needed to provide efficient haptic feedback. Moreover, the needle rotation about its axis is impossible, even though it is an interesting feature to perform bevel tip steering and compensate for needle bending (Webster et al. 2006).

The measurement of needle insertion force is generally obtained with conventional robots with a force sensor directly connected to the needle hub. However, the corresponding systems are generally not adapted to clinical procedures, but rather to simulation (DiMaio and Salcudean 2003) or force modeling (Okamura et al. 2004; Washio and Chinzei 2004). Existing needle drivers using pneumatic actuation are not force-feedback teleoperated: they are only image-guided and not instrumented in order to measure forces. However, the lack of force measurement in robotic needle drivers is not surprising. Measuring insertion forces with a device dedicated to clinical percutaneous procedures requires compliance with several demanding constraints, including the limited available space for the needle driver and the use of standard needles of varying sizes.

In this paper, we focus on the design of a needle driver with force feedback that can be mounted on top of the CT-Bot system (Maurin et al. 2004, 2008). On the one hand, the proposed solution is compatible with the specifications imposed by interventional radiology and CT scanner use. On the other hand, it addresses the issue of insertion force measurement. The motion transmission and the force measurement capability are the original contributions of this work.

This paper is organized as follows. In Section 2, the specifications of a device compatible with force feedback are listed which leads to the proposal of a novel needle-driving principle based on successive grasping and translations of the needle. The mechanical design of the needle driver is presented. Then, the original design of the needle grasper is discussed and detailed in Section 2.4. The resulting prototype is presented in Section 2.5. In Section 3, teleoperated *in vivo* needle insertions are performed on swine with force feedback to validate the proposed device. Finally, the contributions of this work are summarized and future directions are given in the conclusion.

2. Needle Driver Design

To solve the problem of needle steering and force measurement we present in this section a novel device that mimics the manual gesture usually performed. The insertion device grasps the needle on the barrel and then translates to perform insertion or extraction. This operating principle enables a direct force measurement scheme since the needle grasping and its displacement are performed using separated means. This working principle was first developed in a particular form (Piccin et al. 2005) and was then enhanced and improved. It should be noted that under clinical conditions needle retraction is not an essential feature for the needle driver since the practitioner can carry out the needle extraction manually without image guidance.

2.1. Design Requirements

First, the requirements for a needle driver are presented. It is assumed that the entry point and the insertion axis are known and supplied by a positioning device to which the needle driver is connected. The main functional characteristics for a robotized percutaneous therapy scenario are summarized in Figure 3, which presents the working principles used to fulfill the requirements. In Figure 3, the sequence of functions on a path proceeding from left to right (respectively from right to left) answer the question “How is the function to its immediate left performed?” (respectively “Why is the next function performed?”).

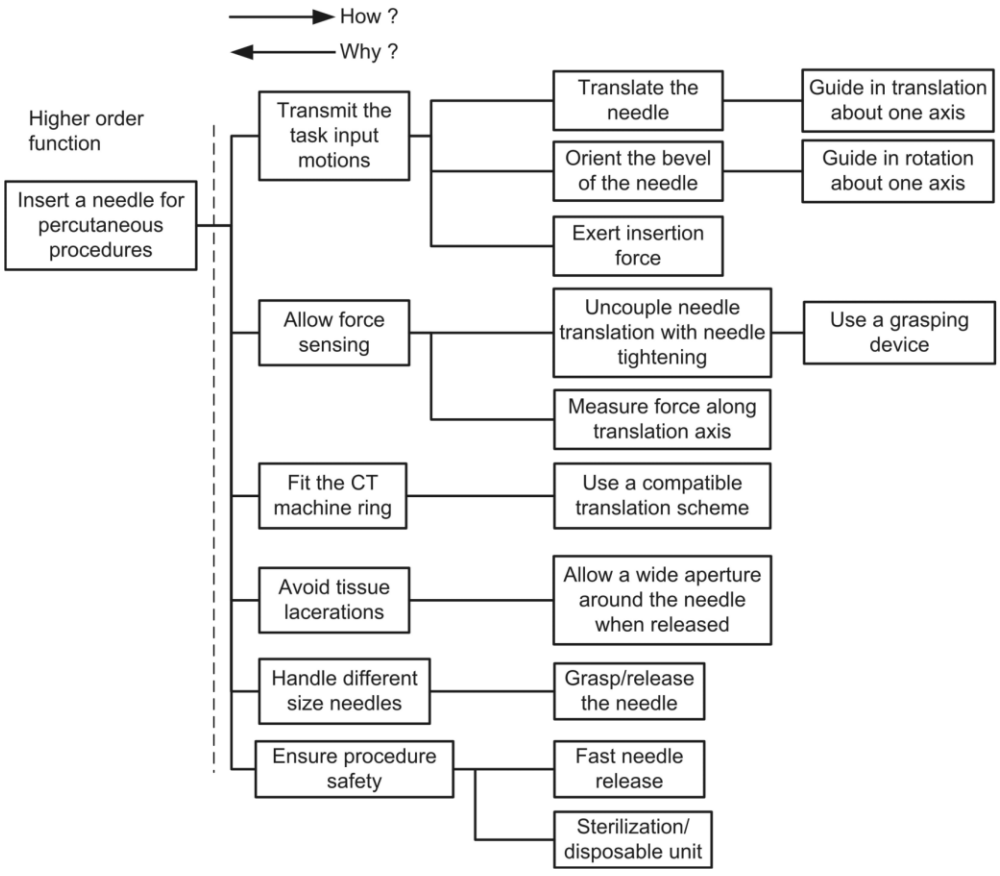

Fig. 3. Functional diagram of the needle insertion device.

2.2. Proposed Working Principle

The needle driver must fit within the bore of the CT scanner, that is, between the patient and the top of the scanner ring. To perform the large needle translation in the limited available volume, the translational movement should be split into a sum of elementary translations. These elementary displacements are obtained using translations of a carriage holding a grasping device and the alternate clamping of the chuck. Compared with previously developed insertion devices (e.g. Piccin et al. (2005)), the needle is manipulated by a single chuck since its distal tip is initially pre-inserted at an entry point on the patient's skin. A small skin incision is made at the entry point to facilitate the needle insertion task that can be described as indicated in Figure 4. With the carriage in its upper position and the chuck opened the needle is first placed in the chuck and pre-inserted at the selected entry point. Then, the chuck is tightened on the needle (Figure 4(a)). The insertion cycle is divided into four steps:

1. the carriage is translated to its lower position (Figure 4(b));

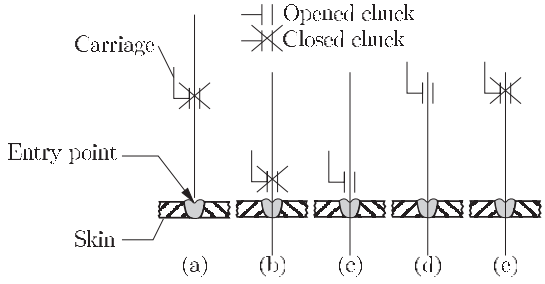

Fig. 4. Insertion cycle carried out with a chuck.

2. the chuck is loosened allowing the needle to move in accordance with motion of internal organs (Figure 4(c));
3. the carriage is translated back (Figure 4(d));
4. the chuck on the carriage tightens again (Figure 4(e)).

The insertion cycle is carried out until the required insertion length is reached. The needle extraction is performed similarly except that the carriage stands initially in its lower position.

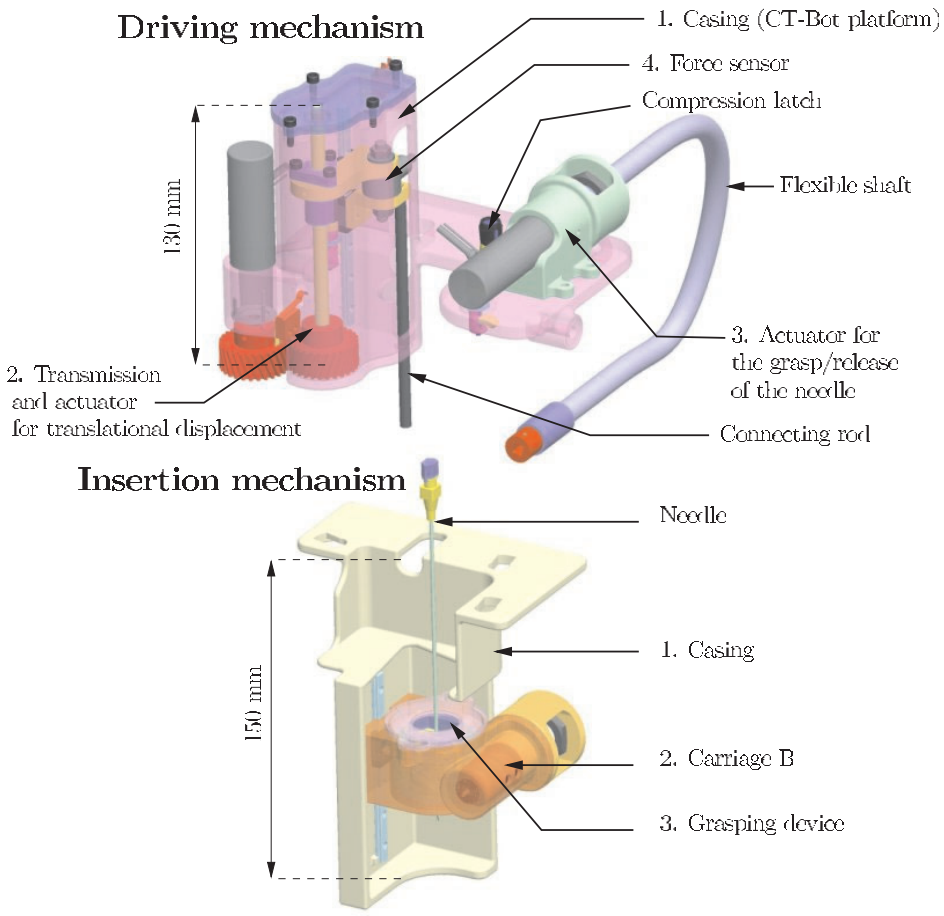

Fig. 5. Exploded view of the needle insertion driver.

Note that, provided that the chuck yields a wide opening, the presented insertion scheme allows free motion of the needle about the entry point induced by the displacement of internal organs.

2.3. Mechanism Overview

The needle driver presented on the exploded view of Figure 5 is made from two main subassemblies. (i) The first is attached to the CT-Bot platform and comprises the actuators and sensors of the insertion device. This first subassembly is referred to as the driving mechanism. (ii) The second includes mainly a grasping device for the needle. This second subassembly is referred to as the insertion mechanism. The first subassembly comprises active components such as actuators and sensors whereas the second only includes passive devices such as the grasping mechanism. Motion transmission between these two subassemblies is obtained using a connecting rod and a flexible shaft. This embodiment addresses the medical requirement of sterilization in which the active parts of the system can be wrapped in sterile bags whereas the passive component can be sterilized and used as a disposable unit.

The driving mechanism is made up of a casing constituted by the CT-Bot platform embedding the transmission and the actuator for the translational displacement of the needle. The driving mechanism also comprises a sensor dedicated to force measurement during needle insertion. The actuator used for the grasp/release of the needle is located on the platform. The insertion mechanism is composed of a casing holding a linear guideway onto which a carriage is connected. A grasping device is mounted on this carriage. Figure 6 provides detailed views of the driving mechanism and the insertion mechanism. The driving mechanism is composed of a rotary motor, M_1, driving a first carriage, A, via a transmission formed by a couple of helical gears and a screw mechanism. A force sensor connects the carriage A to a second carriage A′ mounted on the same rail and holding a connecting rod whose distal end can be temporarily fixed to the carriage B of the insertion mechanism. As such, the connecting rod transmits axial forces from the carriage B holding the needle to the force sensor. The in-

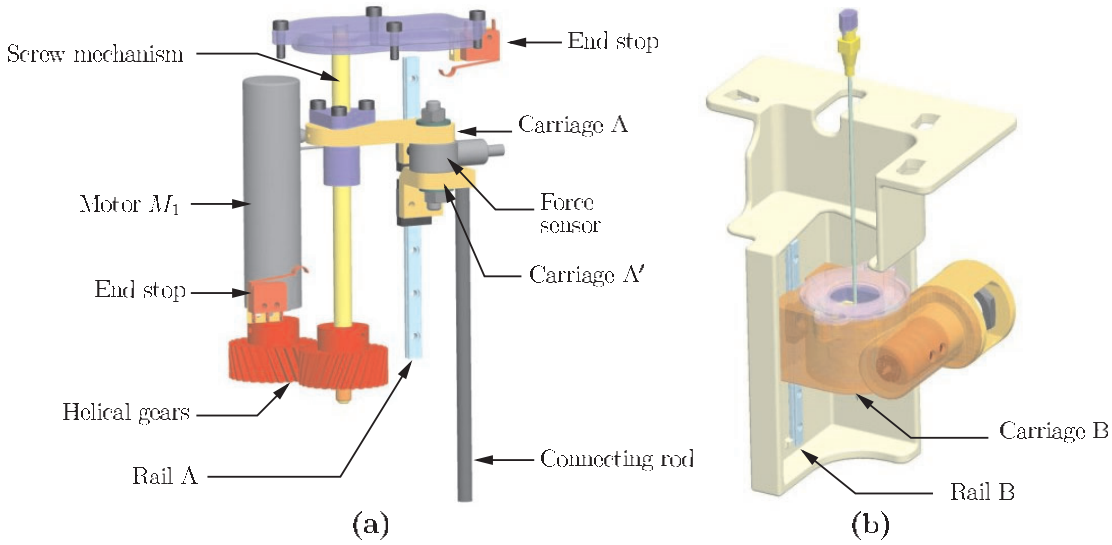

Fig. 6. Detailed views of (a) the driving mechanism and (b) the insertion mechanism.

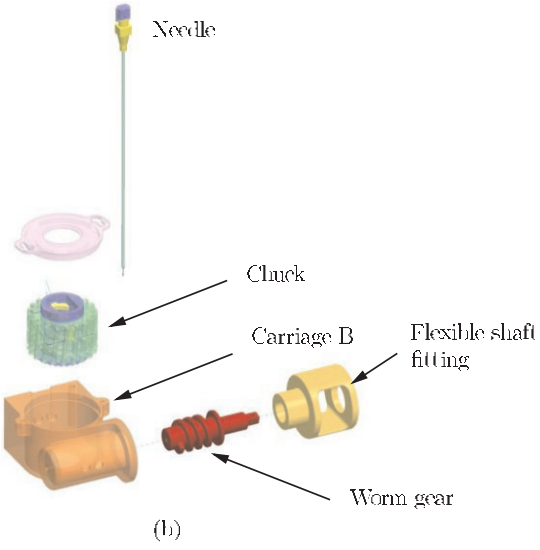

Fig. 7. Exploded view of the carriage B.

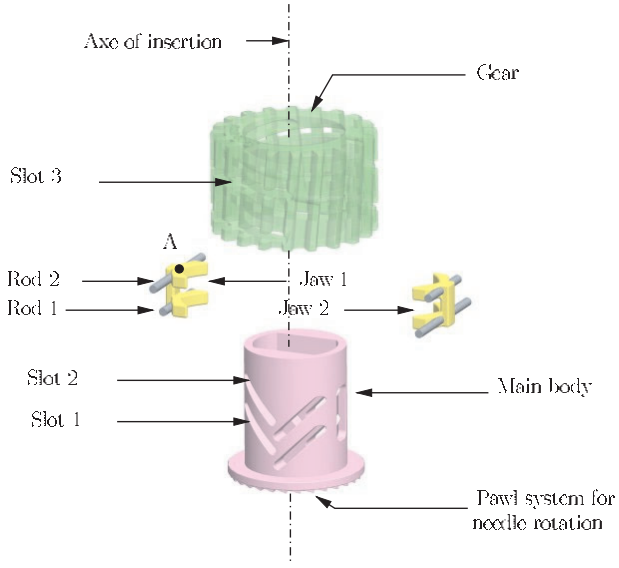

Fig. 8. Exploded view of the chuck.

sertion mechanism can be easily separated from the driving mechanism by releasing three compression latches attached to the CT-Bot platform. An exploded view of the carriage B is presented in Figure 7. It is composed of a casing holding the needle grasping device (a chuck) operated by a worm gear driven via the flexible shaft.

2.4. Chuck design

The main design objective was to provide a grasping device capable to perform on-demand grasp and release of needles of various sizes. Furthermore, the grasping device should allow the needle to move freely when opened and simultaneously have a reduced overall size. The proposed chuck is composed of a main body, two jaws, two pairs of rods and a gear as described in Figure 8. During the tightening of the chuck, the displacement of each jaw is a translation along the direction followed by the rods 1 and 2 inside the slots 1 and 2 on the main body. Simultaneously, each chuck is driven by the slots 3 constructed within the bore of the gear and followed by the rods 2 (which are longer than the rods 1) when the gear is ro-

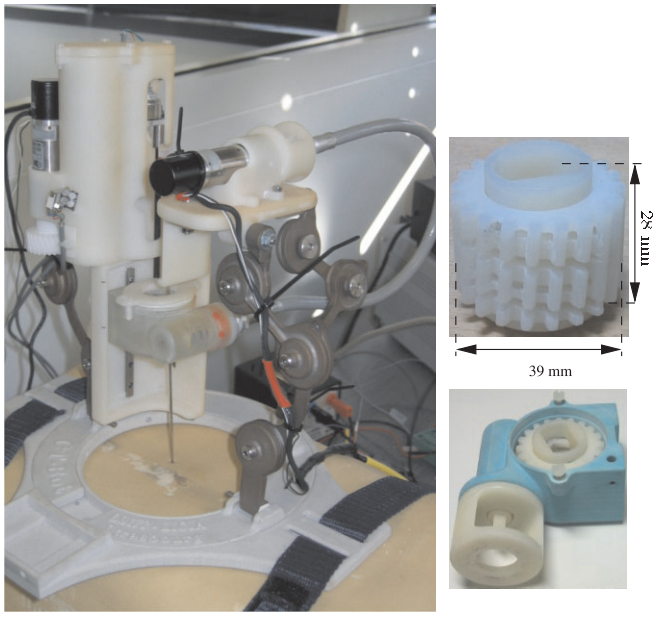

Fig. 9. Fabricated prototype of the insertion device, the chuck and the carriage.

tated about its axis. A pawl system located at the bottom of the main body blocks the rotation of the main body when the gear is operated to open the jaws. Conversely, when grasping a needle with an opposite sense of rotation of the gear, the pawl system allows the main body and the grasped needle to rotate simultaneously. This embodiment allows the needle to rotate about its axis to orient the needle bevel with no additional actuator and provides a security against clamping overload.

2.5. Prototype

A prototype of the needle insertion device has been constructed to carry out *in vivo* experiments. Figure 9 depicts the complete insertion device mounted as a tool on a passive positioning system which can set a predefined incidence for the needle. Most of the parts were obtained using rapid prototyping with an ABS-like resin including the chuck and its associated carriage.

2.5.1. Carriage Translation Capabilities

As depicted in Figure 10 the transmission of the driving mechanism allows the conversion of the rotary input motion generated by a harmonic drive servo into a translational position x_t of the carriage supporting the force sensor. A harmonic drive servo actuator PMA-5a was selected with a 80 : 1 reduction. Based on the equilibrium equation of the system, the maximum force exerted by the carriage is

$$F_C = \frac{\eta}{\lambda}\tau_m$$

where η, λ and τ_m denote the estimated mechanical advantage, the pitch of the screw and the rated output torque of the motor. Numerical values of the prototype lead to $F_C = 1{,}466\tau_m$ which gives a theoretical maximum force of the order of 500 N, which is large enough for the application. Note that this value is different from the maximum insertion force exerted by the needle. This point is discussed in Section 2.6.

2.5.2. Grasping Device Capabilities

The grasping device including the chuck is composed of the elements presented in Figure 11. The rotation of the harmonic drive servo is transmitted via the flexible shaft to a worm gear mechanism acting on the gear of the chuck. The rotation of this latter gear causes the opening or closing of the jaws measured as a radial distance x_j. The grasping force generated by two opposing jaws on a shaft can be related to the driving torque exerted by the motor as

$$F_j = \frac{\eta}{2n}\tau_m$$

where n denotes the transmission ratio. For a driving torque $\tau_m = 0.1$ N · m, the clamping effort exerted by each jaw is approximately equal to 67 N, a sufficient value for the application.

Thanks to its specific design, the presented chuck offers a wide opening which enables the needle to move about the entry point within a cone of opening φ and avoids the risks of tissue laceration between two insertion phases. When the opened chuck is its lower position the needle can move freely in any direction approximately 10° off its central position. The best configuration for needle release is when the carriage is in its lower position. Figure 12 depicts the cone-shaped needle evolution zone for the two extreme positions of the carriage.

2.6. Safety Issues and Needle Insertion Device Specifications

For the considered application, safety is the primary concern during the design process. As underlined by Taylor et al. (1995), non-backdrivable transmissions for patient-interacting devices provide safer designs. For the carriage translation, this construction choice leads to a theoretical maximum force exerted by the carriage of the order of 500 N. However, during experiments the maximum force exerted by the needle has not exceeded 20 N since the insertion force is limited by the friction occurring between the needle barrel and the jaws thus providing an inherently safe behavior. Along the same line, the

Fig. 10. Block diagram of the driving mechanism.

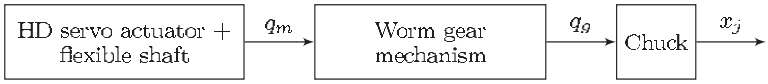

Fig. 11. Block diagram of the grasping mechanism.

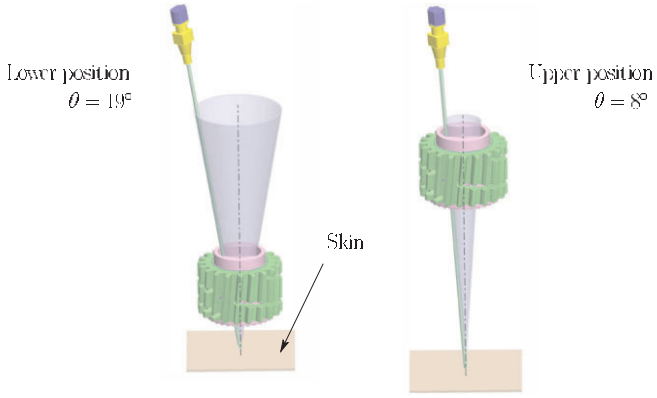

Fig. 12. Free motion of the needle for two carriage positions.

Table 2. Needle insertion driver specifications.

Specification	Value
Mass of the insertion driver	760 g
Maximum insertion stroke	61.8 mm
Maximum travel speed	5.5 mm s^{-1}
Maximum chuck opening	16 mm
Theoretical maximum clamping force	67 N
Maximum insertion force (with a 18-gauge biopsy needle)	20 N

force sensor measurements or the motor current signals can also provide useful information to stop the insertion motion safely.

As explained in Section 1, the supporting five-degrees-of-freedom robot is first positioned and oriented in the free space to provide the correct incidence for the needle insertion. Then, on the fixed supporting robot, the needle insertion device is controlled to perform the insertion task with only one degree of freedom which reduces the complexity of the safety issue significantly. The fact that the robot and its needle insertion tool are mounted on the patient also provides a safe and simple solution to compensate partially for patient's external motions. However, during percutaneous procedures, physicians generally ask their patient to hold their breath for a few seconds during the insertion of the needle. This is required to limit the effects of respiratory motions on internal organs, avoid tissue laceration and improve targeting accuracy. Between two successive insertion phases, the patient resumes breathing and the needle must be released to allow its free motion around the entry point. This important characteristic is provided by the specific designed chuck which offers a 16 mm opening. Finally, the main features of the constructed prototype are summarized and presented in Table 2.

3. *In vivo* Experimental Results

3.1. Experimental Setup

The experimental setup used to evaluate the teleoperated needle insertion is presented in Figure 13. The slave manipulator is composed of the needle insertion device mounted on a passive parallel structure which is attached to an anesthetized swine by straps. This structure is similar to that of the CT-Bot which is not used here for convenience, as the insertion is not performed in the CT-scanner room but in a conventional operating room. Actually, only force feedback (that is, the originality of our paper) is emphasized here. The master manipulator, referred to as the CT-Master, is a linear haptic device designed to meet the prescribed constraints of interventional radiology. In particular, it has a needle-like interface to the operator hand and thus can be seized as a conventional needle (Barbé et al. 2007b). For a more comfortable setup, the main casing of the CT-Master can be tilted by changing the position of the knob present on the left-hand side of the CT-Master as shown in Figure 13(b). The needles used during experiments are classical 18-gauge, 152.4-mm long biopsy needles.

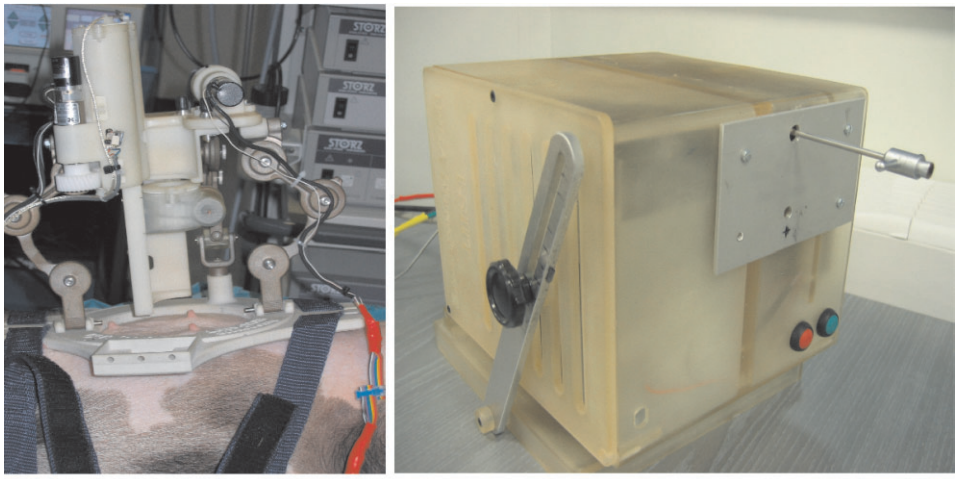

(a) (b)

Fig. 13. Experimental setup: (a) needle insertion device, the slave manipulator mounted on an anesthetized swine; (b) CT-Master, the master manipulator.

3.1.1. Real-time Control and Supervision Software

The control architecture is composed of:

- a control PC, based on a real-time Linux operating system (Xenomai); this PC, dedicated to the control of the motors, is equipped with DAC/ADC cards and counter interfaces; the control software is based on a generic open-source control software developed in our laboratory;
- a PC dedicated to the supervision of the force-feedback teleoperation and potentially to the use of the positioning robot HMI (Maurin et al. 2004).

This decoupled architecture offers a good solution to the issue of X-ray exposure: while the robot and its control unit are in the CT-scan room, the medical staff can supervise the intervention remotely behind a transparent protective screen. The communication between these two PCs is achieved by a serial link dedicated to these experiments to reduce the latency and data loss.

3.2. Bilateral Control Scheme

A force-feedback teleoperation system is useful to enable the operator to sense and manipulate in remote sites. The objective in bilateral teleoperation is to perform the best possible immersion of the operator. This can be characterized by the optimum trade-off between transparency and stability, whatever the interactions with the environment or the human operator. To reach ideal transparency, the mechanical design must exhibit very limited friction and low inertia. Likewise, the choice of the control scheme and its optimal tuning are determined. The mechanical designs of the master (Barbé et al. 2007b) and of the slave manipulators were performed in order to limit friction and inertia as much as possible. Owing to the required forces (up to 15–20 N) and because of technological limitations in direct-drive linear actuators, it is however difficult to perform translations without motion transformations. Rotating motors and transmissions were chosen or designed in order to have the lowest possible friction. Finally, the slave manipulator has non-backdrivable transmission. Although this lack of backdrivability is a drawback from a teleoperation control point of view, it is highly desirable for safety reasons because the slave robot is in direct contact with the patient, as pointed out in Section 2.6. Indeed, this kind of transmission increases both the precision and stiffness, but also prevent problems when the device is not enabled or in the event of a power failure.

The motor used to drive the needle is velocity-controlled which allows the disturbance caused by the tissue interaction to compensated for (the local velocity control loop is faster than the soft tissue dynamics). Then, the forces resulting from the contact are not considered and a simple position control of the slave manipulator can be implemented. Moreover, since the operator exhibits a more damped and stiffer behavior than that of the environment, a three-channel bilateral controller with force environment compensation can be used, as suggested by Hashtrudi-Zaad and Salcudean (2002). The position control loop at the master side is used to modify its dynamics. Simultaneously, the force control loop implemented at the master side increases force-feedback trans-

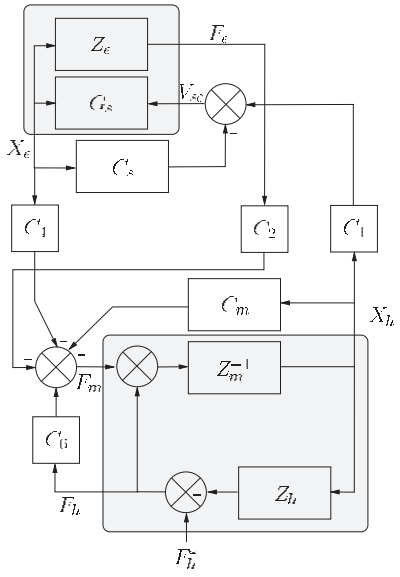

Fig. 14. Three-channel bilateral control scheme used in the experiments.

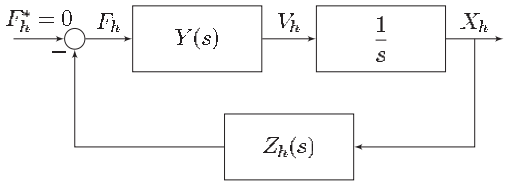

Fig. 15. Simplified bilateral control scheme for stability analysis.

parency. Figure 14 presents the implemented bilateral control scheme.

It is assumed that the operator and the environment interact respectively with the master and the slave manipulators and that they are respectively modeled by the impedances Z_h and Z_e. The impedance Z_m represents the master manipulator model. The position $X_h = X_m$ is the Cartesian position of the operator arm which is also the position of the master manipulator. The force F_h is the interaction force between the master manipulator and the operator. The block G_s is the transfer function of the slave relating the control signal V_{sc} and the slave position X_s. The position $X_e = X_s$ is the Cartesian position of the environment in contact with the needle tip. The block C_6 is the local force feedback controller, C_m and C_s are the local position controllers, respectively for the master and the slave. The blocks C_1, C_2 and C_4 are the three-channel transfer functions. In the experiments, we chose the following controllers:

$$\begin{aligned} C_1 &= C_s = 7.0, \\ C_2 &= 1 + C_6 = 0.15, \\ C_4 &= -C_m = 0.05. \end{aligned} \tag{1}$$

3.2.1. Stability Analysis

In this section the stability analysis of the proposed bilateral control scheme is discussed. The operator's arm dynamics are non-linear and depend on several physiological and environmental factors, but are generally assumed as passive. During needle insertion, the environment can be modeled by a spring-damper system (Barbé et al. 2007a) and characterized by the following model in the Laplace domain:

$$Z_e(s) = K_e + B_e s, \tag{2}$$

where K_e and B_e denote bounded parameters verifying

$$\begin{aligned} 0 \le K_e \le 150 \quad (\mathrm{N \cdot m^{-1}}), \\ 0 \le B_e \le 25 \quad (\mathrm{Ns\ m^{-1}}). \end{aligned} \tag{3}$$

The theory of passivity is classically used to analyze the stability of bilateral control scheme in force-feedback teleoperation (Hogan 1989). The main property of the passivity is that the connection of two passive systems results in a passive system which is therefore stable (Colgate and Hogan 1988). As the human operator is a passive system, the stability of the teleoperation system depends on the passivity of the one-port network composed by the master–slave manipulator and the environment described by Equation (2). This one-port network will be referred to as the MSE system. A one-port network system is said to be passive when its transfer function has no pole in the right-hand s-plane and a positive real part of its complex gain (Colgate and Hogan 1988).

The teleoperation scheme depicted in Figure 14 can be simplified as presented in Figure 15. Under the assumptions on controllers (1) and the notation of Figure 14, the MSE system is represented by the admittance $Y(s)$ as follows:

$$Y(s) = \frac{V_h}{F_h} = \frac{Z_m^{-1} C_2 (1 + C_s G_s)}{1 + C_s G_s + Z_m^{-1}(C_m + C_2 Z_e C_s G_s)}. \tag{4}$$

The numerical models are given in the appendix. The properties of the system have been analyzed numerically with the values of the controllers given in the previous section by sampling the parameters domain. Figure 16 shows the poles of $Y(s)$ (Figure 16(a)) and the real part of the $Y(j\omega)$ for all ω (Figure 16(b)) for the set of environment's parameters given by (3). As the poles of $Y(s)$ are not located in the right-hand s-plane and $\Re(Y(j\omega)) \ge 0$ for all ω, the MSE system is passive and the whole teleoperation system is stable for the specified environment.

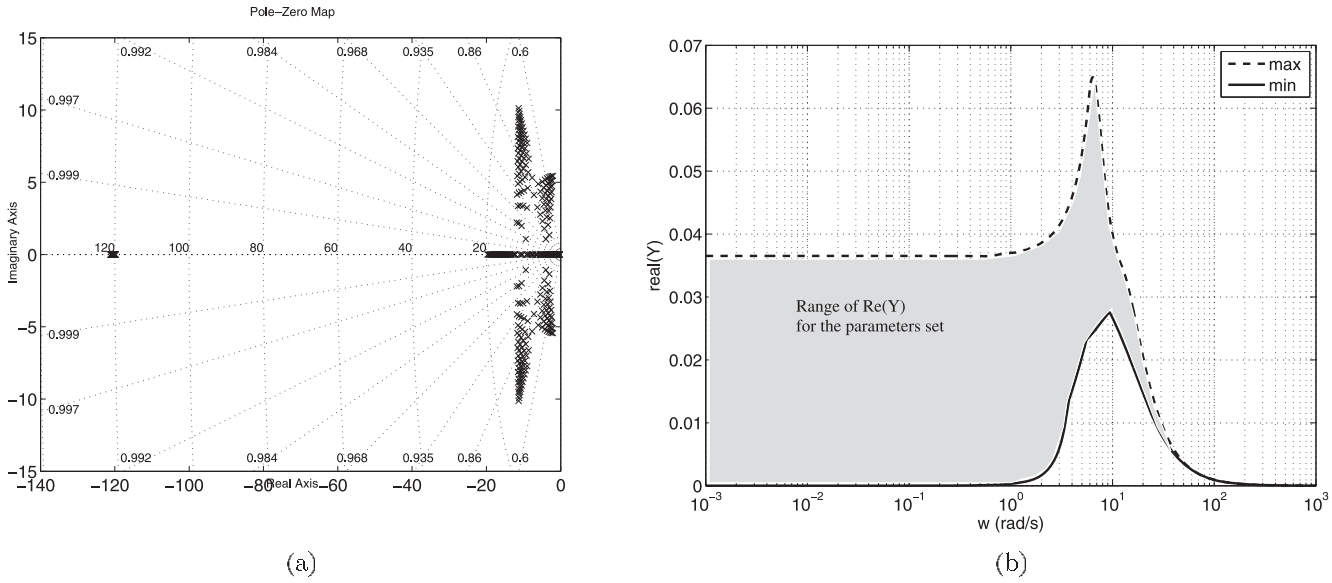

Fig. 16. (a) Poles of $Y(s)$ and (b) the range of the real part of $Y(j\omega)$ for the set of environment's parameters.

3.3. Experimental Results

3.3.1. One-stroke Continuous Teleoperated Needle Insertion

First, we have performed a one-stroke continuous insertion motion in the abdomen of the swine in order to check the efficiency of the teleoperation device. A small incision was made at the needle entry point, as is usually done in interventional radiology to limit the effects of skin rupture. During this experiment the needle was first inserted to a depth of 54 mm using a single motion of the carriage, since the system stroke is 61.8 mm, then the needle was extracted manually. The results of this experiment are presented in Figure 17.

The first two plots in Figure 17 represent the force and the position tracking between the master and the slave. After the grasping of the needle that occurs at time $t = 2.5$ s, the needle insertion teleoperation begins. As already explained in the literature (Okamura et al. 2004; Barbé et al. 2007b), at the beginning of the insertion, the needle pushes the tissue surface which becomes deformed. Then, the needle insertion into the skin is a combination of cutting, friction and compression. During this phase, the force felt by the user is very similar to the force measured at the slave side. When the needle tip position is 29.2 mm, at $t = 28.4$ s, a rupture occurs, possibly the puncture of a muscle or a fascia. It causes an abrupt decrease of the force from -6.35 to -1.8 N. This sudden change in the force profile leads to a fast variation of the remote user's hand position (approximately 10 mm in 0.25 s). Barbé et al. (2007a) presented a method to limit this undesirable effect. It is based on a rupture detection algorithm and an associated event-based teleoperation strategy. In the current work, this strategy is not used. However, the design of the slave does not allow such a very fast variation of position to be followed, as shown in Figure 17. As a consequence, the slave manipulator behaves like a low-pass filter on the position tracking: high accelerations are not transmitted from the master to the slave. In fact, for a medical application, this behavior is advantageous to ensure patient safety. As a result, during this transient phase the position tracking error increases up to 8.3 mm, which has no consequence on the success of the insertion. After this transient phase, the needle progress continues until the position 54 mm, at $t = 37$ s. Then, the chuck is opened and the needle is extracted manually.

The two plots at the bottom of Figure 17 present the root mean square (RMS) force and position tracking errors. Except during the tissue rupture, these errors are very limited. The mean value of the RMS force tracking error is 0.22 N and the standard deviation is 0.16 N, for a force amplitude ranging from -6.3 to 0.2 N. During the most rapid force variations, at $t = 28.4$ s, a transient error up to 1.6 N can be measured. The mean value of the RMS position tracking error is 0.28 mm, with a standard deviation of 0.75 mm. Note that a possible sliding of the needle with respect to the jaws cannot be detected in the position tracking. This phenomenon is rather limited here since force intensity remains relatively low. It could offer an interesting development of the study, in the case of higher force levels. Nevertheless, one should note that needle sliding cannot be dangerous for the patient. Moreover, it would be corrected by the CT-image acquisition performed to check whether the targeting is satisfactory.

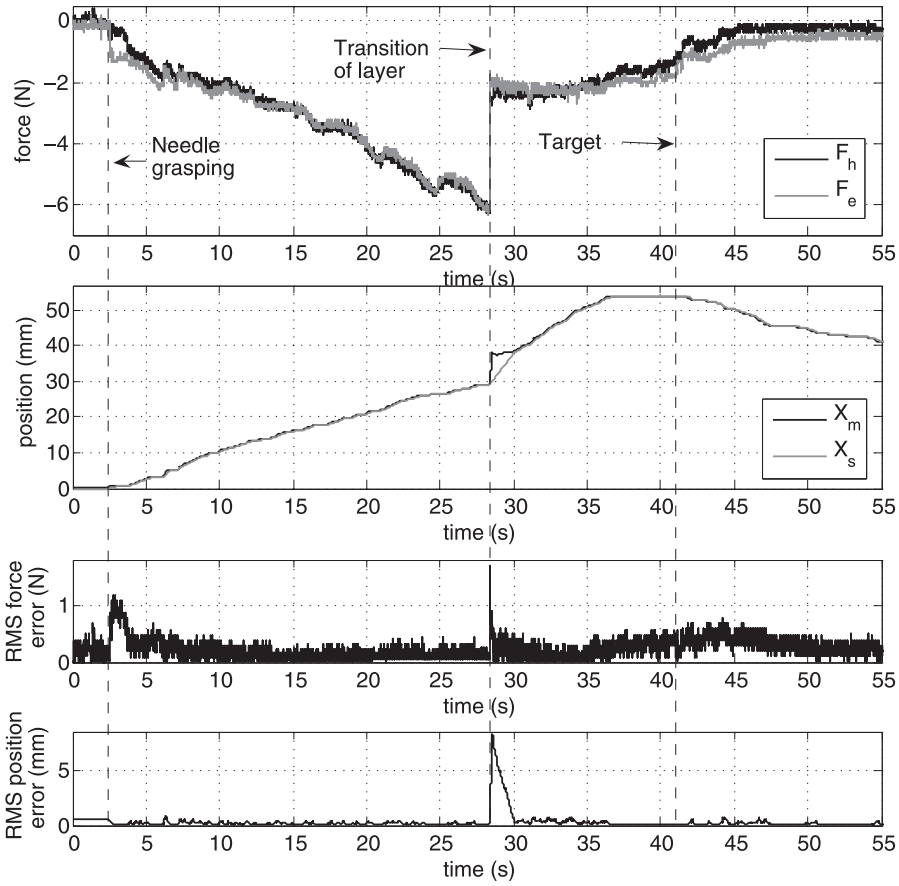

Fig. 17. Continuous needle insertion experiment. From top to bottom: force and position tracking for the master and the slave robots; RMS force and position tracking errors.

3.3.2. Sequential Teleoperated Needle Insertion

In this experiment, the needle insertion device was placed on the swine's abdomen to insert the needle into the liver. A small incision of the epidermis was made at this entry point to facilitate insertion. To reach the desired depth of approximately 100 mm, two insertion cycles are required (see Figure 4). Figure 18 presents the results obtained for such an insertion. The first two plots represent force and position tracking between the master and the slave. The other two plots give the evolution of the RMS tracking errors.

The main phases and events of this insertion are represented by letters, from A to G. At time $t_A = 3.1$ s the needle is grasped and the operator begins the insertion. Then, during the needle insertion, three tissues layers are punctured positioned at 13.6, 27.4 and 54.7 mm when their ruptures occur. These tissues or fascia ruptures correspond to discontinuities in the force profile at $t_B = 12.7$ s, $t_C = 19.5$ s and $t_D = 33.0$ s, respectively. When the carriage of the needle driver reaches its lower position at a position of 61.8 mm (letter E in the figure), the operator hand is constrained by an adequate virtual fixture to remain in its current position, while the carriage goes back to the upper position, which is reached at point F. Then a second insertion cycle begins. Once the needle has reached the position 117 mm, at point G, the operator stops the insertion and releases the needle: the chuck is opened and the needle is extracted manually.

During the insertion, RMS force tracking error is always under 0.5 N, except:

- during the cycle between points E and F;
- when the needle creates a layer rupture at points B, C and D;
- when the chuck grasps the needle at point A.

The maximum force error is 3.9 N, between points E and F. It corresponds to a phase when the slave carriage travels backward and is no longer tracking the master. While artificial force feedback is applied to the master in order to block the operator hand, no force is measured at the slave side, which explains the difference between F_h and F_e. As a result, RMS error mean

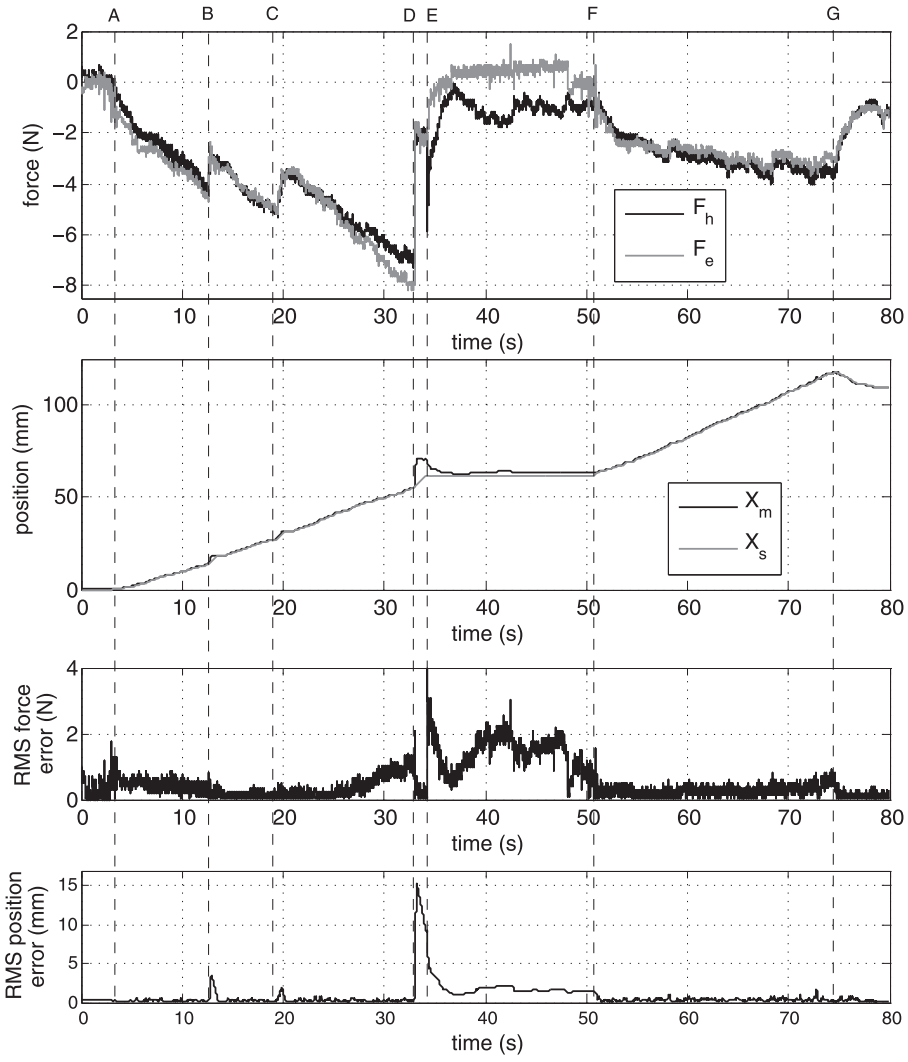

Fig. 18. Sequential needle insertion experiment. From top to bottom: force and position tracking between the master and the slave robots; RMS force and position tracking errors.

values over the whole experiment are not significant. Similar observations can be formulated for position tracking error. The error increases rapidly when the needle penetrates the tissues and during the cycle mode, with a maximum at 15.35 mm.

4. Conclusions and Future Work

CT-scanner interventional procedures are used widely for medical diagnosis and treatment, but the repeated exposure of the physician to X-rays limits the possible number of interventions. To increase the protection of medical staff and the gesture accuracy we have developed an X-ray-compatible teleoperated needle insertion system.

In this paper, the design of a novel needle insertion device has been presented. The proposed needle insertion device is capable of handling standard surgical needles of various sizes and complies with force feedback. In order to ensure patient safety and enable direct force acquisition, the grasping and the motion of the needle are operated separately. The grasping of the needle is performed by a specific chuck which offers a wide opening to avoid tissue laceration when the needle is not being actively inserted. The complete teleoperation system used during *in vivo* tests comprises a master manipulator (the CT-master, a dedicated haptic interface for needle insertion) and a slave manipulator (the needle insertion device used as tool mounted on a passive positioning system). *In vivo* experiments conducted on an anesthetized swine consisting of several remote needle insertions with haptic feedback were car-

ried out and yielded encouraging results that validate both the concept and design of the proposed system. The insertion device and the teleoperation structure proved to be adequate to meet the stated constraints of grasping capabilities and force-reflection for safe needle insertions.

Continuations of this work will include the integration of the presented tool on the robotic positioning device to perform teleoperated percutaneous procedures inside a CT scanner. More elaborate control scheme including an extended use of force-sensor measurements and motor current signals would provide the physician with valuable information to enhance the rendered force feedback and add fail-safe features to the insertion device.

Future perspective also includes the detection of needle sliding using an exteroceptive vision system combined with the force and position measures.

Appendix: Stability Analysis models

The transfer functions of the models and controllers used to analyze the stability of teleoperation scheme are:

- master

$$Z_m^{-1}(s) = \frac{X_h(s)}{F_m(s) + F_h(s)} = \frac{1}{0.24s^2 + 4.10s} \qquad (5)$$

  where $F_m(s)$ and $F_h(s)$ denote respectively the master force control and the interaction force between the master and the human operator;

- slave

$$G_s(s) = \frac{X_e(s)}{V_{sc}(s)} = \frac{1}{s(1 + \tau s)} \qquad (6)$$

  where $V_{sc}(s)$ represents the slave control with a time constant $\tau = 7.8 \cdot 10^{-3}$.

The values of the transfer functions parameters were obtained by an identification using a pseudo-random binary sequence.

Acknowledgments

This work is supported by the Alsace Regional Council and the French National Center for Scientific Research (CNRS). The authors wish to express their sincere appreciation to the IRCAD team for assistance with experiments.

References

Barbé, L., Bayle, B., de Mathelin, M. and Gangi, A. (2007a). *In vivo* model estimation and haptic characterization of needle insertions. *The International Journal of Robotics Research*, **26**(11–12): 1283–1301. http://ijr.sagepub.com/cgi/content/abstract/26/11-12/1283.

Barbé, L., Bayle, B., Piccin, O., Gangloff, J. and de Mathelin, M. (2007b). Design and evaluation of a linear haptic device. *Proceedings IEEE International Conference on Robotics and Automation*. Roma, Italy.

Barrett, S. R. H., Hanumara, N. C., Walsh, C. J., Slocum, A. H., Gupta, R. and Shepard, J. O. (2005). A remote needle guidance system for percutaneous biopsies. *Proceedings of the ASME International Design Engineering Conferences*, Long Beach, CA.

Cleary, K., Melzer, A., Watson, V., Kronreif, G. and Stoianovici, D. (2006). Interventional robotic systems: applications and technology state-of-the-art. *Minimally Invasive Therapy*, **15**(2): 101–113.

Colgate, J. and Hogan, N. (1988). Robust control of dynamicaly interacting systems. *Internationl Journal of Control*, **48**(1): 65–68.

DiMaio, S. and Salcudean, S. (2003). Needle insertion modeling and simulation. *IEEE Transactions on Robotics and Automation*, **5**(19): 864–875.

Hashtrudi-Zaad, K. and Salcudean, S. (2002). Transparency in time-delayed systems and the effect of local force feedback for transparent teleoperation. *IEEE Transactions on Robotics and Automation*, **18**(1): 108–114.

Hogan, N. (1989). Controlling impedance at the man/machine interface. *Proceedings IEEE International Conference on Robotics and Automation*, pp. 1626–1631.

Hong, J., Dohi, T., Hashizume, M., Konishi, K. and Hata, N. (2004). An ultrasound-driven needle-insertion robot for percutaneous cholecystostomy. *Physics in Medicine and Biology*, **49**(3): 441–455. http://stacks.iop.org/0031-9155/49/441.

Kettenbach, J., Kronreif, G., Figl, M., Fürst, M., Birkfellner, W., Hanel, R., Ptacek, W. and Bergmann, H. (2005). Robot-assisted biopsy using computed tomography-guidance: initial results from *in vitro* tests. *Investigative Radiology*, **40**: 219–228.

Maurin, B., Bayle, B., Piccin, O., Gangloff, J., de Mathelin, M., Doignon, C., Zanne, P. and Gangi, A. (2008). A patient-mounted robotic platform for CT-scan guided procedures. *IEEE Transactions on Biomedical Engineering*, **55**(10): 2417–2425.

Maurin, B., Gangloff, J., Bayle, B., de Mathelin, M., Piccin, O., Zanne, P., Doignon, C., Soler, L. and Gangi, A. (2004). A parallel robotic system with force sensors for percutaneous procedures under CT-guidance. *Proceedings of the International Conference on Medical Image Computing*

and Computer Assisted Intervention, Saint-Malo, France, pp. 176–183.

Okamura, A., Simone, C. and O'Leary, M. (2004). Force modeling for needle insertion into soft tissue. *IEEE Transactions on Biomedical Engineering*, **51**(10): 1707–1716.

Patriciu, A., Petrisor, D., Muntener, M., Mazilu, D., Schär, M. and Stoianovici, D. (2007). Automatic brachytherapy seed placement under MRI guidance. *IEEE Transactions on Biomedical Engineering*, **54**(8): 1499–1506.

Piccin, O., Renaud, P., Barbé, L., Bayle, B., Maurin, B. and de Mathelin, M. (2005). A robotized needle insertion device for percutaneous procedures. *Proceeedings of the ASME International Design Engineering Technical Conferences*. Long Beach, CA.

Rösch, J., Keller, F. and Kaufman, J. (2003). The birth, early years, and future of interventional radiology. *Journal of Vascular Interventional Radiology*, **14**: 841–853.

Shoham, M., Burman, M., Zehavi, E., Joskowicz, L., Batkilin, E. and Kunicher, Y. (2003). Bone-mounted miniature robot for surgical procedures: concept and clinical applications. *IEEE Transactions on Robotics and Automation*, **19**(5): 893–901.

Stoianovici, D., Cadeddu, J. A., Demaree, R. D., Basile, H. A., Taylor, R. H., Whitcomb, L. L. and Kavoussi, L. R. (1997). A novel mechanical transmission applied to percutaneous renal access. *ASME Dynamic Systems and Control Division*, **61**: 401–406.

Stoianovici, D., Cleary, K., Patriciu, A., D.Mazilu, Stanimir, A., Craciunoiu, N., Watson, V. and Kavoussi, L. (2003). AcuBot: a robot for radiological interventions. *IEEE Transactions on Robotics and Automation*, **19**(5): 927–930.

Taillant, E., Avila-Vilchis, J., Allegrini, C., Bricault, I. and Cinquin, P. (2004). CT and MR compatible light puncture robot: architectural design and first experiments. *Proceedings of thew International Conference on Medical Image Computing and Computer Assisted Intervention*, Vol. 3216, Saint-Malo, France, pp. 145–152.

Taylor, R., Funda, J., Eldridge, B., Gomory, S., Gruben, K., LaRose, D., Talamini, M., Kavoussi, L. and Anderson, J. (1995). A telerobotic assistant for laparoscopic surgery. *IEEE Engineering in Medicine and Biology*, **14**: 279–288.

Washio, T. and Chinzei, K. (2004). Needle force sensor, robust and sensitive detection of the instant of needle puncture. *Proceedings of the International Conference on Medical Image Computing and Computer-Assisted Intervention*, Saint-Malo, France, pp. 113–120.

Webster, R. J., Kim, J. S., Cowan, N. J., Chirikjian, G. S. and Okamura, A. M. (2006). Nonholonomic modeling of needle steering. *The International Journal of Robotics Research*, **25**(5–6): 509–525. http://ijr.sagepub.com/cgi/content/abstract/25/5-6/509.